

# Ultrafast formation of the benzoic acid triplet upon ultraviolet photolysis and its sequential photodissociation in solution

Chunfan Yang,<sup>1</sup> Hongmei Su,<sup>1,a)</sup> Xuezhong Sun,<sup>2</sup> and Michael W. George<sup>2</sup>

<sup>1</sup>Beijing National Laboratory for Molecular Sciences (BNLMS), State Key Laboratory of Molecular Reaction Dynamics, Institute of Chemistry, Chinese Academy of Sciences, Beijing 100190, China

<sup>2</sup>School of Chemistry, University of Nottingham, University Park NG7 2RD, United Kingdom

(Received 4 January 2012; accepted 9 May 2012; published online 30 May 2012)

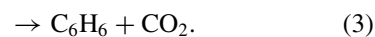
Time-resolved infrared (TR-IR) absorption spectroscopy in both the femtosecond and nanosecond time domain has been applied to examine the photolysis of benzoic acid in acetonitrile solution following either 267 nm or 193 nm excitation. By combining the ultrafast and nanosecond TR-IR measurements, both the excited states and the photofragments have been detected and key mechanistic insights were obtained. We show that the solvent interaction modifies the excited state relaxation pathways and thus the population dynamics, leading to different photolysis behavior in solution from that observed in the gas phase. Vibrational energy transfer to solvents dissipates excitation energy efficiently, suppressing the photodissociation and depopulating the excited  $S_2$  or  $S_3$  state molecules to the lowest  $T_1$  state with a rate of  $\sim 2.5$  ps after a delayed onset of  $\sim 3.7$  ps. Photolysis of benzoic acid using 267 nm excitation is dominated by the formation of the  $T_1$  excited state and no photofragments could be detected. The results from TR-IR experiments using higher energy of 193 nm indicate that photodissociation proceeds more rapidly than the vibrational energy transfer to solvents and C–C bond fission becomes the dominant relaxation pathway in these experiments as featured by the prominent observation of the COOH photofragments and negligible yield of the  $T_1$  excited state. The measured ultrafast formation of  $T_1$  excited state supports the existence of the surface intersections of  $S_2/S_1$ ,  $S_2/T_2$ , and  $S_1/T_1/T_2$ , and the large  $T_1$  quantum yield of  $\sim 0.65$  indicates the importance of the excited state depopulation to triplet manifold as the key factor affecting the photophysical and photochemical behavior of the monomeric benzoic acid. © 2012 American Institute of Physics. [<http://dx.doi.org/10.1063/1.4722084>]

## I. INTRODUCTION

Benzoic acid is the simplest aromatic carboxylic acid and it can be served as a model compound to demonstrate the photochemical properties of aromatic carboxylic acids which may be different from the aliphatic acids. Such understanding is of fundamental importance to understand including the photochemistry of carboxylic acids and related amino acids.<sup>1–6</sup> The phenyl substitution may change photophysical and photochemical properties of the aromatic carboxylic acids particularly because of the conjugation interaction between the phenyl ring and the carboxylic group in aromatic carboxylic acids. For example, Baba and co-workers<sup>7</sup> found that the monomer benzoic acid emitted phosphorescence alone with a high quantum yield because of efficient intersystem crossing to the triplet state, which is quite different from the aliphatic acids.

Photolysis of benzoic acid in the gas phase has been investigated both theoretically and experimentally.<sup>8–12</sup> CASSCF (complete active space self-consistent field) and DFT (density function theory) methods have been used by Fang and co-workers<sup>8</sup> to calculate the geometric and electronic structures of benzoic acids in their  $S_0$ ,  $S_1$ ,  $S_2$ ,  $T_1$ , and  $T_2$  electronic states. A three-surface intersection

was found to exist among the  $S_1$ ,  $T_1$ , and  $T_2$  states by the state averaged CASSCF calculations. The potential energy profiles for three possible photochemical reaction channels (1)–(3) have also been calculated in the ground and excited states. On the basis of these calculations, different photochemical reaction mechanisms were proposed depending upon the excitation wavelength. The C–O bond cleavage channel (1) was suggested to start from the  $S_1$  or  $T_2$  state and generate the fragments of  $C_6H_5CO$  ( $X^2A'$ ) and OH ( $X^2\Pi$ ) in the ground state. This was predicted to be the most important channel upon 270 nm photoexcitation or even at shorter wavelengths. Meanwhile, the C–C bond cleavage channel (2) forming COOH and  $C_6H_5$  radicals was predicted to proceed from the lowest triplet state  $T_1$  but must overcome a much higher barrier (121.2 kcal/mol), and thus was difficult to occur. The decarboxylation channel (3) was suggested to occur in the ground state and thus do not play a role in the photochemistry of the benzoic acid.



Experimentally, Han and co-workers<sup>10,11</sup> investigated the C–O bond cleavage channel (1) at different ultraviolet

<sup>a)</sup> Author to whom correspondence should be addressed. Electronic mail: hongmei@iccas.ac.cn.

wavelengths by probing the nascent OH photoproduct using the laser induced fluorescence (LIF) technique. The energy threshold for producing OH was obtained and estimated to be 102.5–103.9 kcal/mol, which is in agreement with the calculated potential energy barrier<sup>8</sup> of 102.3 kcal/mol (with respect of the  $S_0$  zero level) for the C–O bond cleavage along the  $T_2$  state. Thus,  $T_2$  state was inferred to be the most probable precursor leading to the C–O bond cleavage when excited at 280–294 nm. This conclusion was subsequently supported by theoretical calculations which predicted that C–O fission mainly occurs at the  $T_2$  state upon photoexcitation at 284–294 nm, whereas at shorter wavelength of 266–284 nm C–O fission from the  $S_1$  state is in competition with the fission from the  $T_2$  state.<sup>12</sup> More recently, Ni *et al.* performed multimass ion imaging experiments<sup>13</sup> and observed the other two photochemical reaction channels (2) and (3), in addition to the well-known C–O bond cleavage channel (1). The relative branching ratios between these channels were measured, showing that 248 nm irradiation leads to mainly the OH elimination, while the photodissociation properties of benzoic acid at 193 nm show significant differences yielding COOH and CO<sub>2</sub> as the major products. Comparisons of the measured branching ratios with those estimated from the Rice–Ramsperger–Kassel–Marcus theory suggested that the photodissociation involves many electronic states, but more evidence is required to identify the electronic state for each dissociation channel.

The detection of the photofragments in previous gas phase photolysis investigations have identified different reaction channels and indicated the complex participation of multiple electronic states in the photochemistry of the benzoic acid. The transient intermediate states have not been detected in the previous gas phase experiments, due to their short lifetime and rapid sequential dissociation. In this paper, we perform benzoic acid photolysis experiments in solution to acquire the knowledge of the transient intermediate states which is key to understanding the photochemical reaction mechanism particularly since solvents can serve as efficient cooling bath and stabilize the hot intermediate states, which makes it possible to capture these transient intermediate states in solution.

Time-resolved infrared (TR-IR) absorption spectroscopy in both the femtosecond and nanosecond time domain has been applied to monitor the photolysis of benzoic acid in acetonitrile solution. We have used a combination of the ultrafast and nanosecond TR-IR measurements to allow both the transient intermediate states and the photofragments to be probed. In addition, the wavelength-dependent photolysis TR-IR experiments at 267 nm and 193 nm were performed in order to help clarifying the photochemical mechanism. The results show that the presence of the solvent molecules play an important role in the way of the deactivation of the excited molecules and lead to different reaction paths in solution from that in the gas phase measurements. The solvent-assisted ultrafast relaxation processes bring the excited  $S_2$ ,  $S_3$  state molecules to the lowest  $T_1$  state with a rate of  $\sim 2.5$  ps. With 267 nm excitation, the photolysis is dominated by the formation of the  $T_1$  excited state and photodissociation pathways are totally suppressed since vibrational energy transfer

to solvents dissipates excitation energy efficiently. Whereas with much excess energy passing the dissociation barrier at 193 nm, photodissociation proceeds more rapidly than the vibrational energy transfer to solvents and C–C bond fission becomes the dominant relaxation pathway as featured by the prominent observation of the COOH photofragments. The photodissociation observed at 193 nm is proposed to occur from highly vibrationally excited state of  $T_1$  formed by relaxation from or intersecting with the initially prepared  $S_3$  excited states.

## II. EXPERIMENTAL

### A. Ultrafast TR-IR measurements

The ultrafast TR-IR apparatus has been described previously.<sup>14</sup> Briefly, the 1 kHz output (800 nm, 100 fs) of a commercial Ti:Sapphire oscillator (MaiTai)/regenerative amplifier system (Spitfire Pro, Spectra Physics) pumps a TOPAS-C OPA (Light Conversion) with a difference frequency generator unit in order to produce tunable mid-IR pulses with a spectral bandwidth of ca. 180  $\text{cm}^{-1}$ . A portion of the IR pulse is reflected onto a single element MCT detector (Kolmar Technology) to serve as a reference, and the rest serves as the probe beam, which is focused and overlaps with the pump beam at the sample position. For ultrafast TR-IR experiments, 800 nm is used to pump a harmonic generator to generate UV pulses (267 nm), and the timing is controlled using an optical delay line. In the experiments on the nanosecond/microsecond timescale, the excitation pulse was provided by a Q-switched Nd:YVO<sub>4</sub> laser (ACE-25QSPXHP/MOPA, Advanced Optical Technology, UK) synchronized to the Spit-fire Pro amplifier. The delay between the pump and probe pulses can be controlled with a pulse generator (DG535, Stanford Research Systems) from 0.5 ns to 100 ms. The broadband transmitted probe pulse is detected with a 128-element MCT array detector.

### B. Nanosecond TR-FTIR measurements

Step-scan, time-resolved Fourier transform infrared (TR-FTIR) absorption spectroscopy is employed to monitor transient species or photoproducts produced at 193 nm photolysis. The Step-scan FTIR spectrometer has been described in detail in Refs. 15 and 16 which comprise a Nicolet Nexus 870 step-scan FTIR spectrometer, an excimer laser (Lambda Physik CompexPro 102F), a pulse generator (Stanford Research DG535) to initiate the laser pulse and achieve synchronization of the laser with data collection, two digitizers (internal 100KHz 16-bit digitizer and external 100 MHz 14-bit GAGE 14100A digitizer), and a personal computer to control the whole experiment. The detector used in the experiment is a liquid nitrogen cooled MCT detector, the AC output of which is amplified by external preamplifier (Stanford Research SR560). The spectra are recorded at 16  $\text{cm}^{-1}$  of resolution.

The 193 nm laser is directed through an iris aperture (1 mm) to modify the energy or beam size and then overlapped with the infrared beam in the flowing cell within the sample compartment of the FTIR spectrometer. The

laser energy after the aperture is 3–4 mJ/pulse. A Harrick flowing solution cell with 2-mm-thick CaF<sub>2</sub> windows (path length: 100  $\mu$ m) is used for the measurements. The closed flowing system is driven by a peristaltic pump (ColeParmer Masterflex) to refresh the sample before every laser pulse.

### C. Transient UV-Vis laser flash photolysis measurements

The triplet kinetics is measured by UV-Vis laser flash-photolysis with a nanosecond flash photolysis setup of Edinburgh LP920 spectrometer (Edinburgh Instruments Ltd.), combined with a Nd:YAG laser (Surelite II, Continuum Inc.) or an excimer laser (Lambda Physik CompexPro 102F). The sample was excited by a 266 nm or 193 nm laser pulse (1 Hz, fwhm  $\sim$ 7 ns). The analyzing light was from a 450 W pulsed xenon lamp. A monochromator equipped with a photomultiplier for collecting the spectral range from 280 to 850 nm was used to analyze transient absorption spectra. Samples were freshly prepared for each measurement. Data were analyzed by the online software of the LP920 spectrophotometer. The fitting quality was judged by weighted residuals and a reduced  $\chi^2$  value.

### D. Sample

Benzoic acid (ACROS ORGANICS, 99%) was used as received. Solvents of acetonitrile-*d*<sub>3</sub> (ACROS ORGANICS, 99.8%) and HPLC grade of acetonitrile were used to obtain desirable spectroscopic windows for the TR-IR measurements.

### E. DFT calculations

Geometries and harmonic vibrational frequencies for all molecules of interest are calculated at the B3LYP/D95(d,p) or 6-31+G(d) level with the GAUSSIAN 03 program package.<sup>17</sup> The solvent effects were simulated by the PCM model. All calculated frequencies are scaled by a factor of 0.98 or 0.96, which are typical for these levels of theory.

## III. RESULTS

### A. Photolysis at 266 nm

Fig. 1(a) shows the steady-state IR spectrum of benzoic acid in acetonitrile-*d*<sub>3</sub> solution. Three IR absorption bands were observed at 1724 cm<sup>-1</sup>, 1603 cm<sup>-1</sup>, and 1583 cm<sup>-1</sup>. The strong band at 1724 cm<sup>-1</sup> is assigned to the C=O stretching and the two weak bands at 1603 cm<sup>-1</sup> and 1583 cm<sup>-1</sup> are from the phenyl vibrations of benzoic acid. These fundamental vibrational frequencies in solution can be compared to those observed for the monomeric benzoic acid in the gas phase (1752 cm<sup>-1</sup>, 1609 cm<sup>-1</sup>, and 1591 cm<sup>-1</sup>) (Ref. 18) and in matrix (1752 cm<sup>-1</sup>, 1606 cm<sup>-1</sup>, and 1590 cm<sup>-1</sup>).<sup>19</sup> Additionally, the characteristic benzoic acid dimer band<sup>18</sup> at 1700 cm<sup>-1</sup> is not visible in the IR spectra, showing that there is negligible amount of dimer present in the benzoic acid solution at the low concentration used in these TR-IR experi-

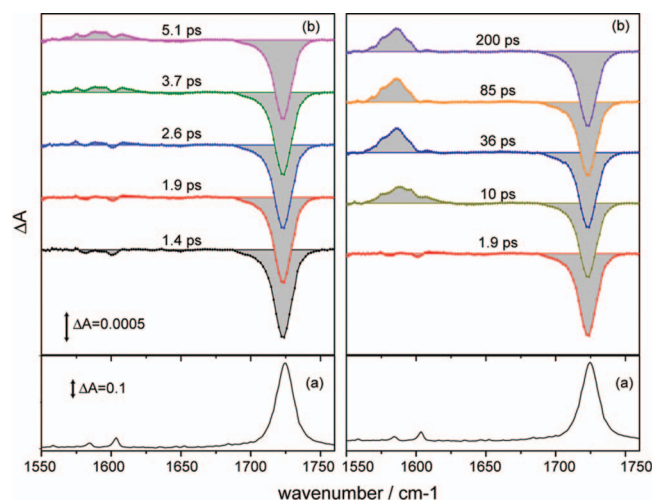


FIG. 1. (a) Steady-state FTIR spectrum of 32 mM benzoic acid in acetonitrile-*d*<sub>3</sub> solution. (b) Transient IR absorption spectra of 32 mM benzoic acid in acetonitrile-*d*<sub>3</sub> solution upon excitation of a femtosecond 267 nm pulse.

ments. This ensures that we are monitoring the photolysis of monomeric benzoic acid and there is no interference from the photochemistry of dimers.

Fig. 1(b) displays the broadband transient IR absorption spectra recorded between 1500 and 1800 cm<sup>-1</sup> after excitation (267 nm) of benzoic acid in acetonitrile-*d*<sub>3</sub>. Following the laser excitation at  $\sim$ 1 ps, the three ground state bands at 1724 cm<sup>-1</sup>, 1603 cm<sup>-1</sup>, and 1583 cm<sup>-1</sup> are instantaneously bleached. Subsequently, a broad positive absorption band at 1586 cm<sup>-1</sup> grows in on top of the two weak bleaching bands of 1603 cm<sup>-1</sup> and 1583 cm<sup>-1</sup>. The two small dips present in the positive band correspond to the 1603 cm<sup>-1</sup> and 1583 cm<sup>-1</sup> bleaching. The positive transient band is featured by a broad lineshape initially at  $\sim$ 10 ps and then becoming narrower due to the vibrational cooling from an initially formed vibrationally hot states.

In transient TR-IR difference spectra, the bleaches monitor the depletion of the ground state molecules, whereas positive signals arise from the vibrational bands of excited states or photoproducts. The 1586 cm<sup>-1</sup> band is not ascribed to the possible photofragments of COOH or C<sub>6</sub>H<sub>5</sub>CO radical which absorb at 1754 cm<sup>-1</sup> or 1828 cm<sup>-1</sup>,<sup>20,21</sup> respectively. To aid assigning this positive band, we calculated vibrational frequencies for the strongest C=O stretching mode of relevant species, respectively at the B3LYP/6-31+G(d) and D95(d,p) level and with the solvent effect simulated by the PCM model. The calculated results are listed in Table I. Compared with the B3LYP/6-31+G(d) results, the D95(d,p) level of calculation predicts more accurate frequencies that are closer to experimental values, for both the S<sub>0</sub> and T<sub>1</sub> states of benzoic acid. The predicted C=O frequency of 1561 cm<sup>-1</sup> for the T<sub>1</sub> state, is in excellent agreement with the experimentally observed peak position of 1586 cm<sup>-1</sup> for the positive band, suggesting that the positive transient band is due to the lowest triplet state of benzoic acid, T<sub>1</sub>, which is of a ( $\pi$ ,  $\pi^*$ ) character.<sup>8</sup>

The possibility of the 1586 cm<sup>-1</sup> band assigned to other transient states, S<sub>1</sub> and T<sub>2</sub>, can be ruled out. According to the theoretically identified electronic structures by Fang and

TABLE I. IR frequency and IR intensity calculated at the B3LYP/6-31+G(d) and D95(d,p) level with the solvent effect simulated by the PCM model. IR extinction coefficients ( $\epsilon$ ) are also listed.

Species	Experimental Observed $\nu(\text{C}=\text{O})$ ( $\text{cm}^{-1}$ )	6-31+G(d)		D95(d,p)		IR extinction coefficient ( $\epsilon$ ) ( $\text{M}^{-1} \text{cm}^{-1}$ )
		$\nu(\text{C}=\text{O})$ ( $\text{cm}^{-1}$ )	IR Intensity ( $\text{KM Mole}^{-1}$ )	$\nu(\text{C}=\text{O})$ ( $\text{cm}^{-1}$ )	IR Intensity ( $\text{KM Mole}^{-1}$ )	
$\text{C}_6\text{H}_5\text{COOH}(S_0)$	1724	1720(1651) <sup>a</sup>	853	1747(1713) <sup>b</sup>	647	743.8 <sup>c</sup>
$\text{C}_6\text{H}_5\text{COOH}(T_1)$	1586	1585(1521) <sup>a</sup>	297	1593(1561) <sup>b</sup>	311	357 <sup>d</sup>
COOH	1730	1828(1754) <sup>a</sup>	520	1835(1798) <sup>b</sup>	448	515 <sup>e</sup>

<sup>a</sup>The harmonic vibrational frequencies in parentheses are scaled by a factor of 0.96.

<sup>b</sup>The harmonic vibrational frequencies in parentheses are scaled by a factor of 0.98.

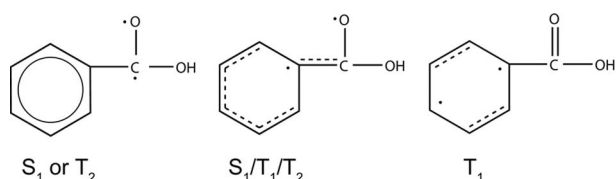
<sup>c</sup>The value is obtained from the steady IR spectrum of benzoic acid in acetonitrile.

<sup>d</sup>The value is estimated according to  $\epsilon(1724 \text{ cm}^{-1}) \times 311/647$ .

<sup>e</sup>The value is estimated according to  $\epsilon(1724 \text{ cm}^{-1}) \times 448/647$ .

co-workers<sup>8</sup> (shown in Scheme 1), both the  $S_1$  and  $T_2$  states correspond to  $(n, \pi^*)$  transition, which means that an electron is promoted from a nonbonding ( $n$ ) orbital to an antibonding ( $\pi^*$ ) orbital. Since  $n$  orbital is located on the carbonyl oxygen, the orbit of the  $S_1$  ( $n, \pi^*$ ) or  $T_2$  ( $n, \pi^*$ ) is then localized primarily in the carbonyl portion of the molecule. For  $T_1$  ( $\pi, \pi^*$ ), on the other hand, the orbit is expected to be more substantially delocalized over the entire aromatic system. So C=O stretching vibration in  $S_1$  ( $n, \pi^*$ ) or  $T_2$  ( $n, \pi^*$ ) state should have much lower frequency than that in  $T_1$  ( $\pi, \pi^*$ ) state because it has a lower double bond character in the  $(n, \pi^*)$  state. In general, there is a larger red shift of at least  $300 \text{ cm}^{-1}$  relative to the ground state molecule when a  $(n, \pi^*)$  state is involved, while a much smaller red shift about  $100 \text{ cm}^{-1}$  is observed in the case of the  $(\pi, \pi^*)$  state.<sup>22</sup> Therefore, the  $1586 \text{ cm}^{-1}$  positive band (with a red shift  $\sim 138 \text{ cm}^{-1}$  relative to the ground state) can be confidently assigned to the  $T_1$  ( $\pi, \pi^*$ ) state, but not  $S_1$  ( $n, \pi^*$ ) or  $T_2$  ( $n, \pi^*$ ) state. Although we extended the probing IR wavelength down to  $1250 \text{ cm}^{-1}$ , no transient species possibly ascribed to  $S_1$  ( $n, \pi^*$ ) or  $T_2$  ( $n, \pi^*$ ) state could be observed in the TR-IR spectra. This is consistent with previous TR-IR experimental results for obtaining the IR spectra of  $(\pi, \pi^*)$  and  $(n, \pi^*)$   $T_1$  excited states.<sup>23,24</sup> The fact that  $T_1$  ( $\pi, \pi^*$ ) state featured by an IR absorption distinctively different from those of  $S_1$  ( $n, \pi^*$ ) or  $T_2$  ( $n, \pi^*$ ) permits the neat detection of these transient states in ultrafast TR-IR spectra, which has turned out to be difficult with the transient electronic spectroscopy due to overlapping triplet and  $(n, \pi^*)$  absorption bands.<sup>25</sup>

Close inspection of the early time dynamics in Fig. 1 reveals that the  $T_1$  absorption band centered at  $1586 \text{ cm}^{-1}$  shows only negligible intensity at times shorter than  $\sim 3.7$  ps, whereas the ground-state bleaching band at



SCHEME 1. The localized pictures of the electronic structures for  $S_1$  ( $n, \pi^*$ ),  $T_2$  ( $n, \pi^*$ ),  $T_1$  ( $\pi, \pi^*$ ), and the  $S_1/T_1/T_2$  three-surface intersection from Ref. 8.

$1724 \text{ cm}^{-1}$  reaches its maximum amplitude at near time zero following the excitation pulse. Such a  $\sim 3.7$  ps time delay in the rise of the  $T_1$  absorption band is indicative of a sequential process for the formation of  $T_1$  state. This is reasonable considering the fact that  $T_1$  cannot be directly populated from the initial  $S_2$  state reached by  $267 \text{ nm}$  excitation, but rather through sequential relaxation pathways, either  $(S_2) \rightarrow (S_1) \rightarrow (T_1)$  or  $(S_2) \rightarrow (T_2) \rightarrow (T_1)$ . According to the El-Sayed propensity rules, the direct intersystem crossing from  $S_2$  ( $\pi, \pi^*$ ) to  $T_1$  ( $\pi, \pi^*$ ) is unlikely to occur. To reach the lowest triplet state  $T_1$  ( $\pi, \pi^*$ ), intermediate states  $S_1$  ( $n, \pi^*$ ) or  $T_2$  ( $n, \pi^*$ ) have to be involved, through  $(S_2) \rightarrow (S_1) \rightarrow (T_1)$  or  $(S_2) \rightarrow (T_2) \rightarrow (T_1)$ .

To analyze the temporal evolution of  $T_1$  state, the band intensity at  $1586 \text{ cm}^{-1}$  is integrated following subtraction of the ground state bleaching from their overlapped spectra. Fig. 2 shows the  $T_1$  absorption band intensity growing as a function of time. After the  $\sim 3.7$  ps time delay, the rise of  $T_1$  can be fitted with a single exponential function satisfactorily, as shown in Fig. 2 insets. The fitting yields a time constant of  $2.5 (\pm 0.5)$  ps, corresponding to the ultrafast population of the triplet state.

Fig. 2 also displays the temporal evolution curves for the ground state bleaching band. Initially,  $267 \text{ nm}$  UV excitation

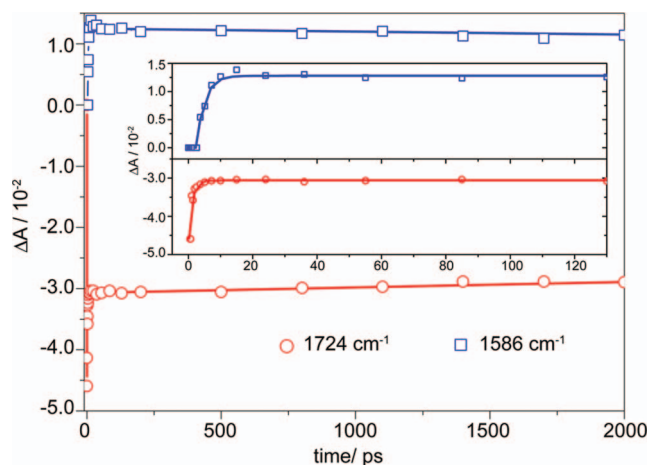


FIG. 2. Representative TR-IR kinetic traces for the  $T_1$  formation at  $1586 \text{ cm}^{-1}$  and ground state recovery at  $1724 \text{ cm}^{-1}$ . Best fitting curves for the kinetics before  $200$  ps are shown in insets by solid lines.

populates the  $S_2$  ( $\pi$ ,  $\pi^*$ ) state, resulting in bleaches at  $1724\text{ cm}^{-1}$  corresponding to ground state vibrations. The bleaching band reaches its maximum amplitude near time zero and partially recovers because of the repopulation from the sequential internal conversion of  $(S_2) \rightarrow (S_1) \rightarrow (S_0)$ . The partial recovery of the bleaching band can be satisfactorily fitted with a single exponential function, as shown in Fig. 2 insets. The fitted time constant of  $\sim 1.8 \pm 0.4\text{ ps}$  corresponds to the overall decay of the  $S_1$  ( $n$ ,  $\pi^*$ ) population.

It is possible that the two sequential relaxation pathways,  $(S_2) \rightarrow (S_1) \rightarrow (T_1)$  and  $(S_2) \rightarrow (T_2) \rightarrow (T_1)$ , may both contribute to the  $T_1$  formation. However, assuming  $T_1$  is formed through the mechanism of  $(S_2) \rightarrow (S_1) \rightarrow (T_1)$ , it would be required that  $S_1$  serves as a reservoir leading to  $T_1$  formation no faster than 3.7 ps after the initial molecular excitation, which is in contradiction with the derived time constant of 1.8 ps for the  $S_1$  decay to  $S_0$ . Therefore, the measured time constants for the  $T_1$  formation and  $S_0$  recovery do not support the mechanism of  $(S_2) \rightarrow (S_1) \rightarrow (T_1)$ . Instead, the second pathway  $(S_2) \rightarrow (T_2) \rightarrow (T_1)$  should be the most plausible mechanism to account for the  $T_1$  formation, based on the following arguments.

Near the vertical excitation of 267 nm ( $\sim 106.8\text{ kcal/mol}$ ), surface intersections of  $S_2$  with  $S_1$  and  $S_2$  with  $T_2$  both occur, as the intersections of  $S_2/S_1$  and  $S_2/T_2$  lie, respectively, 105.4 kcal/mol and 103.3 kcal/mol relative to  $S_0$  according to the *ab initio* calculations.<sup>12</sup> Therefore, it is expected that the initially excited  $S_2$  state can undergo ultrafast branching to populate both the  $S_1$  and  $T_2$  states. This branching must occur within  $\sim 1\text{--}2\text{ ps}$  or less to explain the fast recovery of  $S_0$ . The  $S_1$  state then decays exclusively to  $S_0$  while the  $T_2$  state decays to  $T_1$  only, after a short delay of a further 1–2 ps, perhaps because some vibrational relaxation must take place to access the conical intersection between  $T_2$  and  $T_1$  states. Thus, the further delay caused by the  $T_2$  relaxation to  $T_1$  can account for the observed delayed onset of 3.7 ps for the  $T_1$  formation. Here, the observed ultrafast formation of the  $T_1$  state is presumably due to the heavily intersected potential energy surfaces and thus corroborates the existence of these surface intersections. This is also in line with the previously estimated intersystem crossing rate of  $1.2 \times 10^{12}\text{ s}^{-1}$  from the linewidth of the  $S_0 \rightarrow S_1$  gas phase absorption spectra for the jet-cooled benzoic acid monomer.<sup>26</sup>

It is also noteworthy in Fig. 2 that the ground state bleaching only partially recovers and still sustains 2/3 of the initial intensity at the plateau, indicating that approximately 1/3 of the excited population returns to the ground state and the other 2/3 population is branched to the lowest triplet state  $T_1$ . This leads to an estimated triplet quantum yield of  $\sim 0.67$ . This value is in good agreement with that determined from the  $T_1$  absorption band as follows.

The ultrafast TR-IR spectra (Fig. 1) show characteristic absorption changes due to  $T_1$  formation, from which the triplet quantum yields  $\varphi_T$  can be estimated. The IR absorption intensity for the  $T_1$  spectra ought to be given by

$$\Delta A(\nu) = \Delta \varepsilon(\nu) \times c^* \times d \times \varphi_T.$$

Here,  $c^*$  is the concentration of the initially excited benzoic acid molecules,  $\Delta \varepsilon(\nu)$  is the wavenumber dependent

difference between the IR extinction coefficient of  $T_1$  and  $S_0$  molecules,  $d$  is the path length of the IR cell which is identical (0.1 mm), and  $\varphi_T$  is the triplet quantum yields. The IR extinction coefficients of the relevant species are listed in Table I. The extinction coefficients of the  $S_0$  benzoic acid were obtained from its steady-state FTIR spectra. By comparing the D95(d,p) calculated IR intensities (also listed in Table I) which are proportional to their corresponding extinction coefficients, extinction coefficients of  $T_1$  can be estimated. The concentration  $c^*$  were determined to be  $\sim 5.6\text{ mM}$ , based on the magnitude of the initial ground state bleaching which corresponds to the amount of the initially excited benzoic acid molecules. By this means, the triplet quantum yield  $\varphi_T$  is determined to be  $\sim 0.65$ , which is in excellent agreement with the previously reported value of 0.70 from the phosphorescence measurements of benzoic acid in isopentane-methylcyclohexane rigid glass solution at 77 K.<sup>7</sup> Such a high triplet quantum yield is a characteristic property of the monomeric benzoic acid.

Considering the  $(S_2) \rightarrow (T_2) \rightarrow (T_1)$  relaxation pathway as the most plausible mechanism to account for the  $T_1$  formation, the large triplet quantum yield indicates that the initial branching from  $S_2$  state to  $S_1$  and  $T_2$  is dominated by the relaxation to the triplet manifold, that is, with 65% of population going to  $T_2$ . The remaining 35% of population undergoes branching to  $S_1$  and is followed by a sequential internal conversion to  $S_0$ . Thus, the intersystem crossing from  $S_2$  to  $T_2$  is more competitive, indicating a favorable intersection of  $S_2$  and  $T_2$  states, as suggested by theory<sup>12</sup> to lie at 103.3 kcal/mol relative to  $S_0$ . Intrinsically, the large triplet yield should be ascribed to such favorable surface intersections of triplet excited states with singlet excited states.

In the ultrafast TR-IR spectra, only the ground state bleaching and the  $T_1$  formation were observed, indicating that only photophysical processes occur within 100 ps without any photochemical reactions. The question arises whether the photochemical reactions could take place at longer time scale. Thus, we extended TR-IR measurements to the microsecond time window. As shown in Fig. 3, the transient absorption

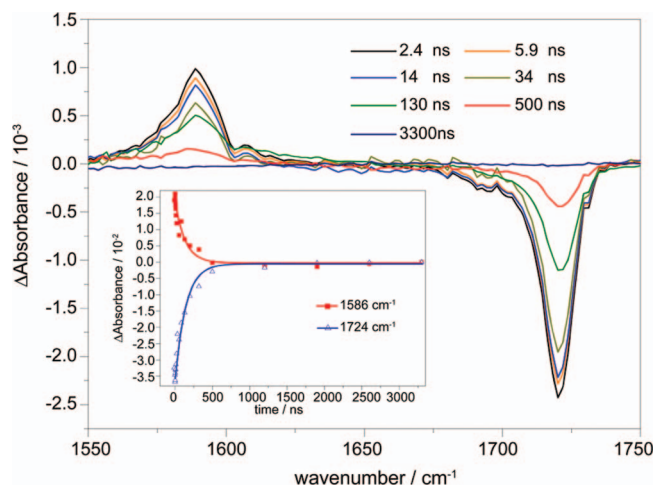


FIG. 3. ns-TR-IR spectra of 32 mM benzoic acid in acetonitrile- $d_3$  solution (without deaeration by  $N_2$ ) following the 267 nm Nd:YVO<sub>4</sub> laser excitation. Insets: Kinetic traces for  $T_1$  decay at  $1586\text{ cm}^{-1}$  and ground state recovery at  $1724\text{ cm}^{-1}$ , along with the fitting shown by solid lines.

bands present at nanosecond and microsecond time scale include only the ground state bleaching at  $1724\text{ cm}^{-1}$  and the positive  $T_1$  band at  $1586\text{ cm}^{-1}$ , which is identical to those observed with the ultrafast TR-IR measurements. The diminishing of the  $T_1$  state with time constant of  $134 (\pm 29)\text{ ns}$  is coincident with the recovery of the ground state bleaching with time constant of  $141 (\pm 15)\text{ ns}$ , which are both ascribed to the intersystem crossing from  $T_1$  to  $S_0$ . Still, the photofragments of COOH and  $C_6H_5CO$  channels detected in gas phase photolysis before<sup>10,13</sup> are not observed in solution. The complete recovery of the ground state bleaching also indicates there is no occurrence of photochemical reactions. It shows here that, from femtosecond to microsecond time scale, the only observed transient species are the  $T_1$  state molecules when benzoic acid is irradiated at 267 nm in solution.

## B. Photolysis at 193 nm

The 193 nm photon does not ionize the solvent acetonitrile or the solute benzoic acid whose ionization potentials are much higher than the photon energy. In addition, the 193 nm irradiation of the pure acetonitrile shows no signals of the expected photofragments CN or secondary products HCN which should absorb strongly in the TR-IR spectra. This ensures that liquid acetonitrile does not undergo photodissociation. Thus, the possible interference from the solvent absorption at 193 nm can be ruled out.

Distinctively different results were obtained upon 193 nm photolysis of benzoic acid solution, with apparent photoproduct formation observed. As shown in the nanosecond time-resolved FTIR absorption spectra (Fig. 4), the ground state bleaching is accompanied by formation of a positive band at  $1736\text{ cm}^{-1}$ . The higher frequency,  $1736\text{ cm}^{-1}$ , of this band precludes its assignment to the excited state species ( $T_1$  or  $S_1$ ,  $T_2$ ), but supports its assignment to the photofragment COOH radical. For COOH radical, our calculation predicts a C = O vibration at  $1754\text{ cm}^{-1}$  at the B3LYP/6-31+G (d) level which coincides with the observed spectral position, although the B3LYP/D95(d,p) calculation made a poorer prediction of  $1798\text{ cm}^{-1}$ . Another possible photofragment,  $C_6H_5CO$  radical, which should absorb strongly at  $1828\text{ cm}^{-1}$  was not observed.

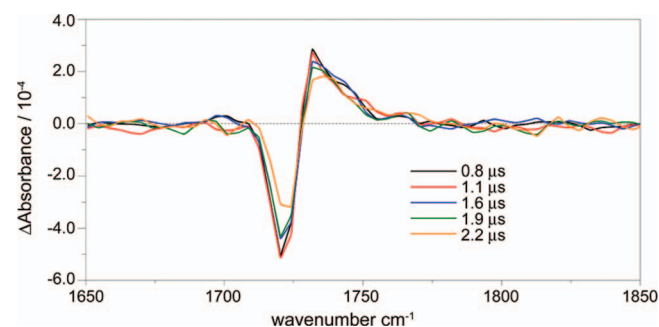


FIG. 4. Step-scan TR-FTIR absorption spectra of 32 mM benzoic acid in acetonitrile- $d_3$  solution obtained following the 193 nm nanosecond laser excitation.

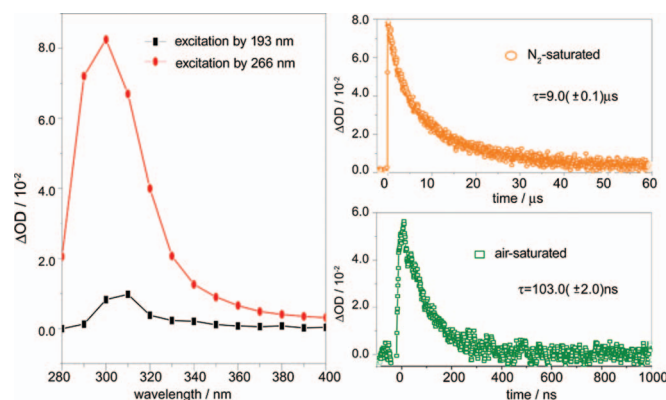
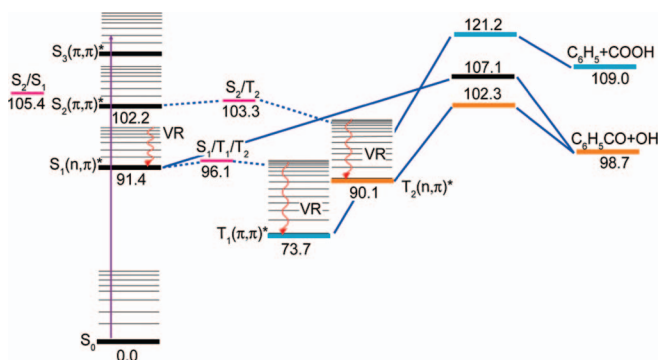


FIG. 5. Transient UV-Vis absorption spectra of benzoic acid in acetonitrile solution obtained following the 266 nm or 193 nm nanosecond laser excitation. The UV absorbance at two wavelengths is adjusted to be identical for comparing the triplet yields. The kinetics traces in  $N_2$  or air-saturated conditions are also shown.

Noticeably, the strong  $T_1$  band at  $1586\text{ cm}^{-1}$  observed with the 267 nm photolysis is not present in the case of 193 nm photolysis. Does this mean that there is no  $T_1$  formation under 193 nm? Given the fact that laser flash photolysis measurements in the transient UV/Vis absorption spectroscopy have higher sensitivity than TR-IR in detecting transient triplet species, we performed further the 266 nm and 193 nm laser flash photolysis transient UV/Vis experiments to examine particularly the triplet formation.

The obtained transient absorption spectra upon 266 nm and 193 nm excitation at their maximum intensity are compared in Fig. 5. For comparing the triplet yields, the UV absorbance of benzoic acid at two wavelengths has been adjusted to be identical, with the solvent absorption of acetonitrile as a background so that the solvent absorption at 193 nm or 266 nm can be deducted. In addition, the measurement at 266 nm and 193 nm used the same pulse energy and the same overlaps with the UV-Vis probing light. Both measures are taken to ensure benzoic acid molecules to absorb the same amount of energy at 266 nm and 193 nm. The observed transient absorption band from 280 nm to 340 nm is characteristic of the  $T_1$  state of benzoic acid, which has a prolonged lifetime of  $\sim 9\text{ }\mu\text{s}$  under  $N_2$ -saturated conditions but quenched to  $\sim 0.1\text{ }\mu\text{s}$  in the presence of  $O_2$ . With the triplet quantum yield  $\phi_T$  at 266 nm estimated to be  $\sim 0.65$  from TR-IR measurements, we can determine  $\phi_T$  of benzoic acid at 193 nm by comparing the triplet absorption intensity in the transient UV-Vis spectra at two wavelengths. The obtained  $\phi_T$  at 193 nm is  $\sim 0.064$ , which is ten times smaller than that of at 266 nm. Such a low triplet quantum yield corroborates the prominent photofragment formation detected in the TR-IR spectra (Fig. 4), suggesting that the excited benzoic acid molecules undergo mainly photodissociation at 193 nm, but not photophysical processes. In fact, the branching ratio for photodissociation channel producing COOH radical turns out to be quite large, which is derived to be  $0.84 \pm 0.26$  by comparing the COOH band intensity with the benzoic acid bleaching band in the TR-IR spectra (Fig. 4) and corrected with their IR absorption coefficients listed in Table I.



SCHEME 2. Schematic excited state relaxation pathways for benzoic acid. Electronic characters of  $S_1$ ,  $S_2$ ,  $S_3$ ,  $T_1$ ,  $T_2$ , the adiabatic transition energies (kcal/mol), transition states for various dissociation channels, dissociation products, and surface intersections of  $S_2/S_1$ ,  $S_2/T_2$ , and  $S_1/T_1/T_2$  are all indicated. All the energy values are adapted from Ref. 8 or Ref. 12.

#### IV. DISCUSSION

Benzoic acid is a bichromophoric molecule with two absorption bands peaked at about 272 nm and 220 nm,<sup>27</sup> which can be assigned respectively to the excitation to the  $S_2$  and  $S_3$  states, on the basis of the calculated vertical excitation energies from the ground state to the three lowest excited singlet states of 113.2, 117.1, and 130.5 kcal/mol along with their respective oscillator strengths 0.0002, 0.015, and 0.1815. Thus, the two excitation wavelengths used in this work, 267 nm and 193 nm, corresponds to the strongly dipole allowed transition to  $S_2$  ( $\pi\pi^*$ ) state and  $S_3$  ( $\pi\pi^*$ ) states, respectively. The  $S_2$  state and  $S_3$  state adiabatically correlate only with (energetically unavailable) highly excited photoproducts and therefore, as no fluorescence is observed, is expected to rapidly relax to the lower lying  $S_1$ ,  $T_2$ , or  $T_1$  state, due to the existence of the surface intersections of  $S_2/S_1$ ,  $S_2/T_2$ ,  $S_1/T_1$ , and  $S_1/T_2$ .<sup>12</sup>

According to previous gas phase photolysis studies, there are several photodissociation relaxation pathways open from the lower lying  $S_1$ ,  $T_2$ , or  $T_1$  state, Scheme 2. The CASSCF calculations<sup>8</sup> predicted that molecules populated to  $S_1$  or  $T_2$  state undergo the C–O bond cleavage producing  $C_6H_5CO$  and OH radicals, corresponding respectively to a barrier height of 107.1 kcal/mol or 102.3 kcal/mol relative to the  $S_0$  zero level, whereas the molecules depopulated to  $T_1$  state are subject to the C–C bond fission yielding COOH and  $C_6H_5$  radicals with a higher barrier of 121.2 kcal/mol above the  $S_0$  minimum. At 266 nm or 248 nm, the photon energy is simply not enough to surmount the C–C bond fission barrier along the  $T_1$  state, so the lower barrier C–O bond cleavage channel was observed to be the major photodissociation pathway.<sup>10,13</sup> When the photon energy is raised to 193 nm, the C–C bond fission becomes dominant whereas the yield of the C–O bond cleavage channel is negligible.<sup>13</sup>

Compared to the gas phase results, our experiments find that the photolysis of benzoic acid in solution behaves quite differently. The 267 nm photolysis is dominated by the  $T_1$  formation with a large quantum yield ( $\phi_T \sim 0.65$ ) and an ultrafast rise time ( $\sim 2.5$  ps), while no discernible photofragments could be observed from femtoseconds until microseconds. Obviously, the photodissociation relaxation pathways are prohibited for the excited benzoic acid molecules in solution.

In solution, the caging effect of the solvent can cause the radical photofragments,  $C_6H_5CO$  and OH, to recombine along the ground electronic state potential energy surface, forming back to the ground state benzoic acid. But this is obviously not the only reason which impedes the photodissociation in solution. Otherwise, there will not be such a large yield ( $\sim 0.65$ ) of  $T_1$  state benzoic acid molecules formed. As we know, another important effect of solvation is solvent-induced energy dissipation, or, vibrational energy transfer to the solvents (vibrational relaxation, denoted with VR in Scheme 2), which can modify the excited state relaxation pathways and thus the population dynamics as discussed below.

The vibrational energy transfer to the solvents usually completes within several picoseconds for polyatomic molecules and thus competes efficiently with the photodissociation which occurs at the same rate. As shown in Scheme 2, for the depopulated  $S_1(v)$  or  $T_2(v)$  molecules surrounded by solvents, in addition to the C–O bond fission, they can be equilibrated to the vibrational zero level  $S_1(0)$  or  $T_2(0)$  by ultrafast vibrational relaxation. Once in the  $S_1$  or  $T_2$  minimum, the molecule cannot break its C–O bond because of the 15.7 kcal/mol or 12.2 kcal/mol of barrier. Thus, by deactivating the excited molecules to the minimum of  $S_1$  or  $T_2$  potential well, vibrational energy transfer to solvents greatly prohibits the photodissociation pathways. Concomitantly, nonradiative decay to lower electronic states becomes dominant. This is particularly the case if considering that the equilibrated molecules in  $S_1$  or  $T_2$  potential well just fall into the proximity of  $S_1/T_1/T_2$  surface intersections,<sup>8</sup> where the subsequent depopulation to  $T_1$  is facilitated. Most excited molecules are deactivated and trapped rapidly to the  $T_1$  state for its deep potential energy well. This is why only the formation of the  $T_1$  state, but no photofragments were observed in the 267 nm photolysis of benzoic acid in solution.

However, when excited with higher energy of 193 nm, the photolysis of benzoic acid in solution is featured by prominent formation of the COOH photofragments and negligible yield of  $T_1$  (lowered to 1/10 of 266 nm). Photodissociation of C–C bond fission becomes the dominant relaxation pathways. This indicates that at higher excitation energy of 193 nm, photodissociation proceeds more rapidly than the vibrational energy transfer to solvents, so the excited molecules are partitioned to the photodissociation pathway (C–C bond fission) instead of relaxation to lower states. Whereas at 267 nm, because the photon energy of 107 kcal/mol just surpasses the energy barrier for the C–O fission along  $S_1$  or  $T_2$  state and lies way below the barrier for the C–C bond fission along  $T_1$  state, the photodissociation rate for neither of C–O fission or C–C bond fission could compete with the vibrational relaxation rate to the  $S_1/T_1/T_2$  surface intersection proximity, where conversion to  $T_1$  becomes dominant and photodissociation pathways are totally suppressed.

Interestingly, our TR-IR spectra shows that only the C–C bond fission channel producing COOH is open with 193 nm photolysis, while another possible channel of C–O cleavage does not occur. If only there is a certain fraction yield of the C–O cleavage channel, its photofragment  $C_6H_5CO$  radical should have been observed because TR-IR is quite sensitive in detecting this radical species which absorbs strongly at

$1828\text{ cm}^{-1}$ .<sup>20</sup> The quantified absolute yield of the C–C bond fission channel at 193 nm,  $\sim 0.84$ , accounts for almost the total of the photochemically depleted benzoic acid molecules. This observation in solution is in agreement with those in the gas phase multimass ion imaging experiments<sup>13</sup> which observed that the photodissociation at 193 nm yielded COOH and CO<sub>2</sub> as the major products. The measured ion intensity ratios of C<sub>6</sub>H<sub>5</sub>:C<sub>6</sub>H<sub>6</sub>:C<sub>6</sub>H<sub>5</sub>CO were 1:1:0.08, corresponding to relative branching ratios of 0.48 for C–C bond fission channel, 0.48 for CO<sub>2</sub> elimination channel, and 0.04 for C–O bond cleavage channel. Without considering the CO<sub>2</sub> elimination channel through S<sub>0</sub> state which is unlikely to occur in solution, the 193 nm photodissociation in the gas phase is actually also dominated by the C–C bond fission channel, while the C–O bond cleavage channel is negligible.

It appears that although the 193 nm photon of  $\sim 145\text{ kcal/mol}$  is high enough to afford both the S<sub>1</sub> or T<sub>2</sub> state C–O bond fission and the T<sub>1</sub> state C–C bond cleavage, the energy favors flowing to the higher barrier C–C bond cleavage channel along the T<sub>1</sub> state. This preference might be due to the much longer lifetime of the T<sub>1</sub> state ( $\sim 0.1\ \mu\text{s}$ ) which allows the photochemical bond cleavage to occur, whereas the intermediate S<sub>1</sub> and T<sub>2</sub> states are simply too short lived to allow any sequential dissociation. Thus, in solution, photodissociation in higher electronic states becomes insignificant due to the competition of ultrafast relaxation, only relatively long-lived lowest triplet state T<sub>1</sub> could possibly result in photodissociation and determine the outcome of the solution photochemistry, provided that the excitation energy is high enough to overcome the T<sub>1</sub> dissociation barrier, which is the case for 193 nm, but not for 267 nm.

Another possibility is that the 193 nm prepared S<sub>3</sub> state may intersect with T<sub>1</sub> state. Similar to T<sub>1</sub>, S<sub>3</sub> state is of a ( $\pi$ ,  $\pi^*$ ) character<sup>12</sup> and the excitation is localized in the aromatic ring, which may also lead to the C–C bond cleavage. Although S<sub>3</sub> state correlate only with (energetically unavailable) highly excited photofragments, the C–C bond dissociation may cross over to the T<sub>1</sub> state at some intersection points, from which the ground state photofragments of C<sub>6</sub>H<sub>5</sub> + COOH are eventually formed. By intersecting with T<sub>1</sub> state, the S<sub>3</sub> state molecules reached at 193 nm could simply bypass the S<sub>1</sub> or T<sub>2</sub> dissociation pathway, leading only to the T<sub>1</sub> state dissociation products of C<sub>6</sub>H<sub>5</sub> + COOH, as observed here and other work.<sup>13</sup> Further excited state *ab initio* calculations are required to establish this model.

By relaxation from or intersecting with the initially prepared S<sub>3</sub> excited states, the highly vibrationally excited T<sub>1</sub> molecules undergo mainly the photodissociation of the C–C bond cleavage. Accordingly, the T<sub>1</sub> yield is found to be significantly lowered at 193 nm. T<sub>1</sub> can be identified as the key intermediate state leading to the C–C bond dissociation channel. This supports previous theoretical prediction<sup>8</sup> that T<sub>1</sub> is the only possible excited state which can lead to the C–C bond dissociation.

From the initially populated S<sub>2</sub>( $\pi$ ,  $\pi^*$ ) state and S<sub>3</sub>( $\pi$ ,  $\pi^*$ ) state, the excited state relaxation is expected to proceed sequentially involving several intermediate states S<sub>1</sub>, T<sub>2</sub>, and T<sub>1</sub>, eventually to S<sub>0</sub> state, as summarized in Scheme 2. According to our measured large T<sub>1</sub> quantum

yield of  $\sim 0.65$ , depopulation to triplet manifold is apparently overwhelming the early excited state relaxation processes, which becomes the key factor affecting the photophysical and photochemical behavior of the monomeric benzoic acid. Indeed, this can be testified by our observation of T<sub>1</sub> formation and C–C bond dissociation along T<sub>1</sub> state in solution photolysis as well as previously observed C–O bond dissociation along T<sub>2</sub> state in the gas phase.

## V. CONCLUSION

Time-resolved infrared absorption spectroscopy in both the femtosecond and nanosecond time domain has been applied to measure the photolysis of benzoic acid in acetonitrile solution at 267 nm and 193 nm, respectively. By combining the ultrafast and nanosecond TR-IR measurements, both the transient intermediate states and the photofragments have been detected, from which the formation rate and fraction yields were determined quantitatively and key mechanistic insights were obtained.

At 267 nm, the photolysis of benzoic acid in solution is dominated by the ultrafast formation of T<sub>1</sub> with a large quantum yield ( $\varphi_T \sim 0.65$ ), while no discernible photofragments could be observed from femtoseconds until microseconds. Different from the gas phase results, the photodissociation relaxation pathways are prohibited in solution because the dissociation cannot compete with the ultrafast vibrational relaxation to the solvent molecules, which brings the S<sub>1</sub> or T<sub>2</sub> molecules to S<sub>1</sub>/T<sub>1</sub>/T<sub>2</sub> surface intersection proximity where the conversion to lower T<sub>1</sub> state becomes dominant. Most excited molecules are simply deactivated and trapped rapidly to the T<sub>1</sub> state for its deep potential well.

At 193 nm, photodissociation of C–C bond fission becomes the dominant relaxation pathways, featured by prominent formation of the COOH photofragments and negligible yield of T<sub>1</sub>. At higher energy of 193 nm, photodissociation proceeds more rapidly than the vibrational energy transfer to solvents, thus allowing the excited molecules partitioned to the photodissociation pathway (C–C bond fission) instead of relaxation to lower states. In addition, it shows that although the 193 nm photon energy is high enough to afford both the S<sub>1</sub> or T<sub>2</sub> state C–O bond fission and the T<sub>1</sub> state C–C bond cleavage, the energy favors flowing to the higher barrier C–C bond cleavage channel along the T<sub>1</sub> state. This preference might be due to the much longer lifetime of the T<sub>1</sub> state which allows sequential dissociation to occur, whereas the intermediate S<sub>1</sub> and T<sub>2</sub> states are simply too short-lived. Or, the S<sub>3</sub> state reached at 193 nm could intersect with T<sub>1</sub> state and bypass the S<sub>1</sub> or T<sub>2</sub> dissociation pathway, leading only to the T<sub>1</sub> state dissociation products of C<sub>6</sub>H<sub>5</sub> + COOH.

Overall, the ubiquitous solvent molecules are shown to play important roles in the deactivation of the excited molecules and lead to different photolysis behavior in solution from that in the gas phase. The solvent-assisted ultrafast relaxation processes bring the excited S<sub>2</sub> or S<sub>3</sub> state molecules to the lowest T<sub>1</sub> state with a rate of  $\sim 2.5\text{ ps}$  after a delayed onset of  $\sim 3.7\text{ ps}$ . Our observation of the ultrafast formation of T<sub>1</sub> state corroborates the existence of the surface intersections of S<sub>2</sub>/S<sub>1</sub>, S<sub>2</sub>/T<sub>2</sub>, and S<sub>1</sub>/T<sub>1</sub>/T<sub>2</sub>, while the measured large

$T_1$  quantum yield of  $\sim 0.65$  indicates the importance of the excited state depopulation to triplet manifold as the key factor affecting the photophysical and photochemical behavior of the monomeric benzoic acid.

## ACKNOWLEDGMENTS

This work is financially supported by the National Natural Science Foundation of China (NNSFC) (Grant Nos. 20973179 and 21073201) and the Chinese Academy of Sciences (CAS). M.W.G. gratefully acknowledges receipt of a Royal Society Wolfson Merit Award. We thank the referees for very helpful suggestions while reviewing this paper.

- <sup>1</sup>S. S. Hunnicutt, L. D. Waits, and J. A. Guest, *J. Phys. Chem.* **93**, 5188 (1989).
- <sup>2</sup>S. S. Hunnicutt, L. D. Waits, and J. A. Guest, *J. Phys. Chem.* **95**, 562 (1991).
- <sup>3</sup>H. T. Kwon, S. K. Shin, S. K. Kim, H. L. Kim, and C. R. Park, *J. Phys. Chem. A* **105**, 6775 (2001).
- <sup>4</sup>P. D. Naik, H. P. Upadhyaya, A. Kumar, A. V. Sapre, and J. P. Mittal, *Chem. Phys. Lett.* **340**, 116 (2001).
- <sup>5</sup>A. Kumar and P. D. Naik, *Chem. Phys. Lett.* **422**, 152 (2006).
- <sup>6</sup>H. M. Su, Y. He, F. N. Kong, W. H. Fang, and R. Z. Liu, *J. Chem. Phys.* **113**, 1891 (2000).
- <sup>7</sup>H. Baba and M. Kitamura, *J. Mol. Spectrosc.* **41**, 302 (1972).
- <sup>8</sup>J. Li, F. Zhang, and W. H. Fang, *J. Phys. Chem. A* **109**, 7718 (2005).
- <sup>9</sup>J. Li and T. B. Brill, *J. Phys. Chem. A* **107**, 2667 (2003).
- <sup>10</sup>Q. Wei, J. L. Sun, X. F. Yue, H. M. Yin, and K. L. Han, *Chem. Phys. Lett.* **448**, 11 (2007).
- <sup>11</sup>Q. Wei, J. L. Sun, X. F. Yue, S. B. Cheng, C. H. Zhou, H. M. Yin, and K. L. Han, *J. Phys. Chem. A* **112**, 4727 (2008).
- <sup>12</sup>Q. Fang and Y. J. Liu, *J. Phys. Chem. A* **114**, 680 (2010).
- <sup>13</sup>Y. A. Dyakov, A. Bagchi, Y. T. Lee, and C. K. Ni, *J. Chem. Phys.* **132**, 014305 (2010).
- <sup>14</sup>P. Brennan, M. W. George, O. S. Jina, C. Long, J. McKenna, M. T. Pryce, X. Z. Sun, and K. Q. Vuong, *Organometallics* **27**, 3671 (2008).
- <sup>15</sup>W. Q. Wu, C. F. Yang, H. M. Zhao, K. H. Liu, and H. M. Su, *J. Chem. Phys.* **132**, 124510 (2010).
- <sup>16</sup>W. Q. Wu, K. H. Liu, C. F. Yang, H. M. Zhao, H. Wang, Y. Q. Yu, and H. M. Su, *J. Phys. Chem. A* **113**, 13892 (2009).
- <sup>17</sup>M. J. T. Frisch, G. W. Schlegel, H. B. Scuseria *et al.* GAUSSIAN 03, Revision B.03, Gaussian, Inc., Wallingford, CT, 2004.
- <sup>18</sup>J. M. Bakker, L. Mac Aleese, G. von Helden, and G. Meijer, *J. Chem. Phys.* **119**, 11180 (2003).
- <sup>19</sup>S. G. Stepanian, I. D. Reva, E. D. Radchenko, and G. G. Sheina, *Vib. Spectrosc.* **11**, 123 (1996).
- <sup>20</sup>X. Z. Sun, S. M. Nikiforov, J. X. Yang, C. S. Colley, and M. W. George, *Appl. Spectrosc.* **56**, 31 (2002).
- <sup>21</sup>C. S. Colley, D. C. Grills, N. A. Besley, S. Jockusch, P. Matousek, A. W. Parker, M. Towrie, N. J. Turro, P. M. W. Gill, and M. W. George, *J. Am. Chem. Soc.* **124**, 14952 (2002).
- <sup>22</sup>M. J. Vanderburgt, A. H. Huizer, C. Varma, B. D. Wagner, and J. Luszyk, *Chem. Phys.* **196**, 193 (1995).
- <sup>23</sup>M. W. George, C. Kato, and H. Hamaguchi, *Chem. Lett.* **22**, 873 (1993).
- <sup>24</sup>T. Yuzawa, C. Kato, M. W. George, and H. Hamaguchi, *Appl. Spectrosc.* **48**, 684 (1994).
- <sup>25</sup>P. M. Hare, C. E. Crespo-Hernandez, and B. Kohler, *J. Phys. Chem. B* **110**, 18641 (2006).
- <sup>26</sup>G. Meijer, M. S. Devries, H. E. Hunziker, and H. R. Wendt, *J. Phys. Chem.* **94**, 4394 (1990).
- <sup>27</sup>V. Talrose, E. B. Stern, A. A. Goncharova, N. A. Messineva, N. V. Trusova, and M. V. Efimkina, "UV/Visible spectra," in *NIST Chemistry WebBook, NIST Standard Reference Database Number 69*, edited by P. J. Linstrom and W. G. Mallard (National Institute of Standards and Technology, Gaithersburg, MD), <http://webbook.nist.gov> 2012.